STING-triggered CNS inflammation in human neurodegenerative diseases

Alex S. Ferecskó (alex.ferecsko@ucb.com)
UCB Pharma (United Kingdom)
Miranda J. Smallwood
University of Exeter
Adrian Moore
UCB Pharma (United Kingdom)
Corin Liddle
University of Exeter
Jia Newcombe
University College London
Janet Holley
University of Exeter
Jacqueline Whatmore
University of Exeter
Nicholas J. Gutowski
University of Exeter
Paul Eggleton
University of Exeter

Article

Keywords: cerebral endothelial cells, cGAS, cortical neurons, neuroinflammation, palmitic acid.

Posted Date: February 14th, 2023

DOI: https://doi.org/10.21203/rs.3.rs-2264071/v2

Abstract

Background: Some neurodegenerative diseases have an element of neuroinflammation that is triggered by viral nucleic acids, resulting in the generation of type I interferons. In the cGAS-STING pathway, microbial and host-derived DNA bind and activate the DNA sensor cGAS, the resulting cyclic dinucleotide, 2'3-cGAMP binds to a critical adaptor protein, stimulator of interferon genes (STING), which leads to activation of downstream pathway components. However, there is limited work demonstrating the activation of the cGAS- STING pathway in human neurodegenerative diseases.

Methods: Post-mortem CNS tissue from donors with multiple sclerosis (n=4), Alzheimer's diseases (n=6) and Parkinson's disease (n=3), amyotrophic lateral sclerosis (n=3) and non-neurodegenerative controls (n=11) were screened by immunohistochemistry for STING and relevant protein aggregates (e.g., amyloid-b, a-synuclein, TDP-43). Human brain endothelial cells were cultured and stimulated with the STING agonist palmitic acid (1-400μM) and assessed for mitochondrial stress (release of mitochondrial DNA into cytosol, increased oxygen consumption), and downstream regulator factors, TBK-1/pIRF3 and inflammatory biomarkers interferon-β release and changes ICAM-1 integrin expression.

Results: In neurodegenerative brain, elevated STING protein was observed mainly in brain endothelial cells and neurons compared to non-neurodegenerative control tissues where STING protein staining was weaker in comparison. Interestingly, higher STING presence was associated with toxic protein aggregates. (e.g., in neurons). Similarly high STING protein levels were observed within acute demyelinating lesions in multiple sclerosis subjects. To understand non-microbial/metabolic stress activation of the cGAS-STING pathway, brain endothelial cells were treated with palmitic acid. This evoked mitochondrial respiratory stress up to a ~2.5-fold increase in cellular oxygen consumption. Palmitic acid induced a statistically significant increase in cytosolic DNA leakage from endothelial cell mitochondria (Mander's coefficient; P <0.05) and a significant increase in TBK-1, phosphorylated transcription factor IFN regulatory factor 3, cGAS, cell surface ICAM. In addition, a dose response in secretion of interferon-b was observed but failed to reach statistical significance.

Conclusions: The histological evidence show that the common cGAS-STING pathway appears to be activated in endothelial and neural cells in all four neurodegenerative diseases examined. Together with the *in vitro* data suggest that the STING pathway might be activated via perturbation of mitochondrial stress and DNA leakage resulting in downstream neuroinflammation hence this pathway may be a target for future STING therapeutics.

Introduction

Most neurodegenerative diseases (NDs) have an element of neuroinflammation that has been speculated to be triggered by viral nucleic acids, resulting in the generation of type I interferons. The cytosolic DNA sensor cyclic GMP–AMP synthase (cGAS), the stimulator of interferon genes (STING) pathway, was initially thought to be activated primarily by viral DNA [1]. However, more recent evidence suggests that

self-DNA can activate the pathway [2] and subsequent production of the cyclic dinucleotide, 2'3-cGAMP binds to the critical adaptor protein STING resulting to the activation and translocation to the trans Golgi network. This leads to recruitment of the interferon inducer – TANK-binding kinase 1 (TBK-1) and phosphorylation of IRF3 and IKK resulting in production of type I interferons (IFNs) and proinflammatory cytokines. There is limited work demonstrating the presence of cGAS-STING activation in primary cells of neurodegenerative CNS tissue. Despite this, the sensing of endogenous DNA and type I IFNs are emerging as important for the development of neurodegenerative diseases. The STING and TBK-1 are implicated in several neurodegenerative conditions and patients showed increased expression of cGAS-STING pathway genes in their neuronal tissues [3-5].

Thus, investigations of cGAS-STING IFN-driven diseases, expanding beyond the more systemic inflammatory and infectious diseases, are more commonly encountered [6, 7]. Indeed, type I IFN production is believed to influence neurodegenerative progression [8]. When the blood brain barrier (BBB) becomes compromised during neuroinflammation, type I IFN can enter the CNS directly [9]. Neurotrophic viruses in the systemic circulation often encounter the first assault of IFN from dendritic cells. If this fails, there is a need for further production of IFN. The requirement for locally produced type I IFNs at the gateway to the BBB and CNS may arise from the necessity to have rapid innate immunity for suppressing viral infections that avoid systemic elimination. There is evidence that human cerebral microvascular endothelial cells - (hCMEC/D3) [10] and CNS cells such as neurons, astrocytes and microglia also produce IFNs [11].

The type I interferons are a group of 14 or more host defence molecules divided into IFN-a and IFN-b subtypes. They have important separate and overlapping roles against viruses and other microbes [12]. In general, cGAS stimulation preferentially elicits an IFN-β response, whereas Toll-like receptor stimulation predominately increases IFN-α expression [13]. Recent studies have implicated type I IFN-dependent signalling as an inflammatory driver in certain NDs [14, 15]. Cellular stress generated by a build-up of toxic protein aggregates in neural and brain endothelial cells can lead to the release of mitochondrial and nuclear dsDNA into the cell cytosol, where it may act as a self-ligand activating the STING agonist γ-interferon-inducible protein (IFI16) and cGAS [16, 17]. Indeed, the expression of STING and cGAS have been demonstrated in human astrocytes and microglial cells [18].

Although other studies have focused on the activation of cGAS-STING in glial cells, there is less information about whether the brain endothelial cells or neurons participate in STING activation. Here we show that in human CNS tissue, robust levels of STING is present and higher in the brain microvascular and neuronal cells of several NDs including Alzheimer's disease (AD), amyotrophic lateral sclerosis (ALS), Parkinson's disease (PD) and multiple sclerosis (MS) compared to non-neurodegenerative samples. Palmitic acid (PA) is a common saturated fatty acid that serves as an energy source, but also can cause lipotoxicity during higher intake over long periods [19]. Also, PA can cause a pro-inflammatory microenvironment, leading to BBB leakage, subsequently entering into the brain and causing harmful effects to neurons and glial cells [20-23]. The precise mechanism of PA-induced damage to the brain is not known. *In vitro* studies suggest that PA can induce α-synuclein accumulation [24], tau

hyperphosphorylation and β-amyloid protein (Aβ) formation [25]. In our study, STING expression occured in close proximity to clusters of neural cells expressing amyloid-b in AD brain, TDP-43 in ALS spinal cord, a-synuclein in PD substantia nigra pars compacta (SnPC) and in acute lesions in the white matter of MS brain. This supports evidence that PA may exerts some of its lipotoxic effects through activation of cGAS-STING pathway. Furthermore, we examined whether human cerebral microvascular endothelial cells (hCMEC/D3) perturbed with the cGAS-STING agonist PA resulted in nuclear/mitochondrial DNA leakage into the cytosol of cells, evoking a cGAS-STING innate immune response. Our results showed that cGAS-STING activation induces the production of IFN-b and increased intercellular adhesion molecule 1 (ICAM-1) expression on hCMEC/D3s.

Materials And Methods

Study Approval and human tissue

Our study used human brain or spinal cord post-mortem tissues from 16 patients with neurological diseases (multiple sclerosis (*n*=4), Alzheimer's (*n*=6) or Parkinson's disease (*n*=3) and spinal cord from amyotrophic lateral sclerosis *n*=3)) and 11 control patients with non-neurological background. Both diseases and control tissues were obtained, with ethical approvals, from tissue banks. A total of 94 sections were immunostained and used for qualitative observations (Supplementary Table 1).

Antibodies and Reagents

For immunoblotting of cGAS-STING and downstream pathway proteins, primary antibodies used were: mouse monoclonal anti-human STING (R&DSystems – MAB7169), rabbit polyclonal anti-human cGAS (Abcam – ab224144), mouse monoclonal anti-human TBK1 (Cell Signalling Technology - #3504), and mouse monoclonal anti-human ICAM-1 (Abcam – ab2213). Appropriate infra-red dye secondary antibodies used were goat anti-rabbit green (LiCor 926-32211 800CW) and goat anti-mouse- green (LiCor 926-32210 800CW). For immunofluorescence analysis of STING distribution in disease and control CNS tissues, sections were probed with a number of primary antibodies including mouse monoclonal anti-human STING (R&DSystems – MAB7169), rabbit anti-human amyloid-b (Abcam – ab2539), rabbit monoclonal anti-human TDP-43 (Abcam – ab109535), rabbit monoclonal anti-human a-synuclein (Abcam – ab209538), mouse monoclonal anti-human calnexin (ThermoFisher – MA3-027). For cell type specific identification and colocalization of STING with distinct neural cell types and brain endothelial cells, the following primary antibodies were used: rabbit anti-human NeuN (Abcam – ab177487), rabbit anti-human GFAP (Thermo Fisher PA5-16291) and rabbit anti-human CD68 (ThermoFisher PA5-32330) and the corresponding secondary antibodies, goat anti-rabbit alexa fluor 488 (ThermoFisher – A-11024) and goat anti-mouse alexa fluor 647 (ThermoFisher – A-21235), (Supplementary Table 2).

PA was purchased commercially for the preparation and treatment of STING pathway agonists experiments on cultured cells (Sigma, PO500). Saturated PA, lipid-containing medium, was prepared by combining PA with bovine serum albumin (BSA). Briefly, PA was dissolved in ethanol to produce a 200 mM solution, and then combined with 20% free fatty acid-free, low-endotoxin BSA (Sigma, 1595) to

produce stock solutions with PA concentrations ranging from 1 to 4 mM. These stock solutions were filter-sterilized and stored at -20°C. Control media containing ethanol and BSA was also prepared. Fresh working solutions were prepared by diluting each stock solution (1:10) in culture medium. The final BSA concentration was kept constant in all PA working solutions, whereas the PA-to-BSA ratio varied with the PA concentrations. All cells tested were cultured and grown to confluency at 4% oxygen in an oxygen-regulated hypoxia chamber (Baker Ruskinn). Cells were then exposed to PA (between 1 & 400 mM) or control media for 16 h.

Histology and immunohistochemistry of human CNS tissues

For immunofluorescent staining, snap-frozen post-mortem brain and spinal cord tissue sections were screened by immunohistochemistry using specific antibody probes for STING, appropriate pathological aggregates of protein (e.g., amyloid-β, α-synuclein or TDP-43), and marker-specific antibodies directed against neural cell types (e.g., microglia: anti-CD68, astrocyte: anti-GFAP and neurons: anti-NeuN). Glass mounted tissue sections (10μm) were rapidly fixed in 4%PFA and incubated with primary and relevant secondary antibodies in PBS at 1:100 concentration. Autofluorescence eliminator (Millipore 2160) was added to the tissue for 5 min and washed off in successive 70 % ethanol washes. Tissue sections were washed, rehydrated, and mounted in anti-quenching fluorescent mounting medium with 4',6-diamidino-2-phenylindole (DAPI - ProLong™ Gold anti-fade mountant, Fisher Scientific, P36931). Coverslips were sealed with nail varnish and stored at 4°C in the dark for subsequent microscopic examination.

Microscopy

Immunofluorescent detection of labelled CNS sections was carried out using Leica DM4000 B LED fluorescence microscope equipped with a black and white digital camera. High-resolution pseudo-colour images were captured using air (20x, 40x) and oil immersion objectives (60x).To assess colocalization between distinct immunosignals, collages of images were captured of each of the three channels over selected areas in cortical grey matter (AD), white matter (MS) or SnPC (PD) and cervical spinal cord (ALS) of both the diseased tissue sections and corresponding control tissue samples. A built-in software algorithm was used to visualize colocalization at cellular level with the aid of specific marker antibodies to distinguish between neural cell types.

To minimize fading of immunofluorescence and therefore altering intensity of the immune signal care was taken to complete micro photographing in one session and to avoid exposing the sections for prolonged periods to UV light or to repeat the capturing process on the same areas of the sections. To estimate the intensity of immunolabelling and provide comparable dataset for qualitative assessment, exposure parameters (illumination strength, exposure time, etc.) were kept constant and preserved throughout the entire image taking process. Image taking was performed only once on a given area to prevent false positive and negative results due to photobleaching and/or overexposure.

Cultured and stained hCMEC/D3 cells were observed and imaged using a Zeiss Elyra 7 lattice structured illumination microscope (SIM; Zeiss Zen Black 3.0), equipped with a Plan-Apochromat 60x/1.4 Oil DIC

M27 objective. The dual PCO edge sCMOS cameras were set to collect 1024 x 1024 pixels for a frame size of 64 x 64µm, which resulted in a pixel scaling of 0.031 µm. Z-stacks with a range of 6-10µm were selected, with an optical section of 90-100nm, which meets nyquist sampling.

The Elyra 7 was configured to use a quad-core main beam splitter (LBF 405/488/561/642), and two different camera filter sets were used for 405 & 488 and 561 wavelengths, respectively (BP 420-480 + BP 495-550 and BP 570-620 + LP 655). Several pre-requisites for accurate colocalization measurements were checked before imaging all treatments. In brief, the dynamic range was set up to be suitable for all treatments (>1000). The image quality was assessed for high noise levels and bleed-through, and the system point spread function (PSFs) was checked to make sure it met specifications, processed images were examined for any significant artefacts.

The sample was excited with a 405 & 488 nm (100 mW) laser and a 561 nm (100 mW) with power set to 20% for all tracks. The SIM imaging parameters were as follows: the number of SIM phases = 13, and the SIM grating periods varied according to the excitation wavelength from 34.0 to 42.0µm.

All images were then SIM processed using standard strength computation settings for fixed samples within Zen black 3.1. Processing was done on an Aquifer HIVE-multicore processing workstation. Background levels of fluorescence were obtained by measuring the mean intensity of each stain outside the cells. Images were then linearly spectrally unmixed (LSU) to remove background and eliminate any cross-talk that the system's main beams splitters and filters had not addressed. LSU was done using automatic two-component extraction (Zeiss Zen Blue 2.3).

Human brain microvascular endothelial cell (hCMEC/D3) culture

The blood-brain barrier endothelial cell line, human cerebral microvascular endothelial cells (hCMEC/D3 cells - VH Bio, UK) was cultured and grown to confluence in rat-tail collagen type I coated (100µg/ml) tissue culture flasks at 37°C and in 4% O_2 /5% CO_2 / nitrogen humid atmosphere. Cells were cultured in MV-2 endothelial cell growth medium, MV supplement Mix (MV-2 - PromoCell, UK) with 10% heat inactivated fetal bovine serum and gentamicin (50 µg/ml). The hCMEC/D3s were used for up to 40 passages. Confluent cells were trypsinized using 0.05% v/v trypsin/EDTA, passaged, and sub-cultured.

Immunoblot analysis for cGAS, STING, TBK-1, Phospho-IRF3 and ICAM-1

Whole-cell protein isolates were collected from hCMEC/D3s using RIPA lysis buffer (Fisher Scientific) at 4 °C with protease inhibitor tablets (10668304, Fisher Scientific), phosphatase inhibitor cocktail (15614189, Fisher Scientific) and analysed by immunoblotting. Samples were electrophoresed on 12 % mini-Protean TGX SDS-polyacrylamide gradient gels (Bio-Rad) in running buffer (25 mM Tris, 192 mM Glycine, 0.1% SDS pH 8.3) at a constant voltage of 75V for 15 min and then 100V for 35–45 min. Separated proteins were transferred to premade trans-blot 0.2 mm nitrocellulose membranes (Bio-Rad) using a Turboblotter (BioRad) at 1.3 mA/25 V for 3 min. Blotted membranes were washed in water, and total protein loading was assessed using Revert™ 700 Total Protein Stain (Li-Cor 926-11010) and imaged using an Azure

Biosystems C500 Infrared imaging system. Blots were incubated in and blocked from non-specific antibody binding with TBST with 3% w/v BSA and 0.1 % v/v Tween for one hour and then incubated overnight at 4 °C with a rabbit polyclonal antibody directed against human cGAS (Abcam ab224144; 1:1000 dilution) or mouse monoclonal antibody against human STING (R&D Systems MAB7169; 1:1000 dilution), or mouse monoclonal anti-human ICAM-1(Abcam ab53013 MEM-11), or rabbit monoclonal antibody directed against human TBK1 (Cell Signaling 3504; 1:1000 dilution) or phosphoIRF3 ser396 (Cell Signaling #4947; 1:1000 dilution – rabbit mAb 4947). After 3 washes in TBS-Tween, (Tris, 20 mM, NaCl, 150 mM, pH7.6 0. 1% v/v Tween), blots were probed with either of two secondary infrared antibodies (green anti-mouse or anti-rabbit) at 1:15,000 diluted in blocking buffer at RT for 1 h. Blots were digitally imaged using a LiCor scanner (Odyssey CLx Imager). Image studio (Li-Cor) software was used to normalize target band intensity from total protein loading images and using lane normalization factors. In addition, a goat anti-rabbit β-actin antibody (Cambridge Bioscience - rabbit A300-485A; 1:3000 dilution or Merck mouse A5316; 1:3000 dilution) was used to confirm equal loading. Immunoblots shown are representative of at least three separate experiments.

For post-transfer protein normalisation measurement, 5 mls Revert™ 700 protein stain (Li-Cor) was added to each blot for 5 mins RT, then washed briefly with (6.7% v/v acetic acid, 30% v/v/ methanol in H_2O). Stained membranes were imaged in the 700 nm channel with an Azure Biosystems C500 Infrared imaging system. The lane with the most protein was given a value of 1 and all others a fraction of that to obtain lane normalisation factor (LNF) = signal for each lane/signal for lane with highest signal. Normalized signal = Target band signal / LNF.

IFN-β detection in hCMEC/D3 supernatants by ELISA

A commercial ELISA assay was purchased from R&D systems (Human IFN-β ELISA, Kit 41410) and employed to measure IFN-β in endothelial cell culture supernatants pre- and post-stimulation with 1-400 mM PA following the manufacturer's instructions.

Detection of cytosolic DNA and mitochondria staining procedures

Cytochemical staining was performed with hCMEC/D3 cells grown in eight-well chamber slides (Lab-Tek 154534). Cytosolic DNA and mitochondria staining in live cells was achieved using the protocol of Ashley and colleagues [26]. A diluted stock of PicoGreen solution (Molecular Probes) at 3 ml/ml was added directly into cell culture medium. The hCMEC/D3 cells were then incubated for 1 h at 37°C, unless stated otherwise, under standard culture conditions. In some experiments, we co-stained hCMEC/D3 cells with the mitochondria selective dye Mitotracker Red CM-H2XRos (Molecular Probes) by adding 100 nM directly to the culture medium and incubating the cells for 2–15 min, followed by incubation in dye-free medium (phenol red free DMEM supplemented with 4.5 g/l glucose and 25 mM HEPES buffer) for a further 20 min. The cells were rinsed three times in pre-warmed PBS and cover slipped. Images were then visualised using Structured illumination microscopy (SIM).

Analysis of real-time extracellular oxygen consumption (OCR)

PA-driven oxygen consumption was analysed using an extracellular oxidation assay kit (Abcam, Cat# ab197243). Exponentially growing cultured hCMEC/D3s ($6x10^4$ cells per well) were seeded in 96-well plates and incubated overnight in 150 mL media in 5% CO_2 at 37°C. Cells were then rinsed twice with 37°C prewarmed fatty acid (FA)-free medium (base measurement medium), then 150 mL PA (range 10, 50, 100, 200 and 400 mM – final concentration), 10 mL extracellular oxygen consumption reagent and FA measurement medium were added to each well without cells and used as signal control. Additional 1 mL (0.625 mM) fatty acid oxidation (FAO) activator, FCCP (Carbonyl cyanide-4-(trifluormethoxy) phenylhydrazone, Abcam - ab120081) was subsequently supplemented into wells as a positive control or 1 mL (2.5 mM - final concentration) antimycin A (Abcam ab141904) as a negative control of cellular respiration. Each well was sealed with 100 mL 37°C prewarmed high sensitivity mineral oil (Abcam ab 197243), taking care to avoid bubbles. Plates were read immediately at excitation/emission wavelengths of 380 nm/650nm at 1.5 min intervals for 30 min in a fluorescence microplate reader at 37°C (SpectraMax M2 - Molecular Devices).

Image Analysis

The image colocalization analysis was conducted in IMARIS 9.9; Menders analysis and regression tests were applied [27]. Briefly, to normalise the images across treatments images were thresholded by selecting a bassline where the red and green channels were most separated. Specifically, the separate tracks thresholds were set to just above their background levels (for an example see Supplementary Fig. 2). Cytosolic pixel intensity analysis was administered by selecting regions of interest on cells cytosol and extracting pixel frequency and intensity information. The intensity information was then normalised between 0-1 to enable comparisons between treatments and plotted as a histogram (an example of how the cytosol ROI was selected see Supplementary Fig. 1).

Statistical Analysis

Statistical ANOVA analyses were performed with GraphPad Prism 6.0 software. Test, group sizes, and P values are given in the corresponding figure legends. P values <0.05 were considered statistically significant. Linear regressions models (LM) were fitted with Rv4.01. For data that indicated a non-normal residual relationship; a nonlinear term was included in the model, i.e. polynomial term.

Data Availability

The data set supporting the conclusion of this article is included within the main article and in the supplementary material. No data generated in this study was downloaded into a public domain.

Results

Identification of areas and characterisation of CNS tissue samples

Standard stains were used to find regions of interest in both pathological and control tissue sections. For the MS tissue samples, oil-red-O staining of myelin was used to identify demyelinating areas of white matter. In normal control tissue, the white matter oil-red-O staining produces an even, pink stain of myelinated tissue matrix. A similar staining pattern is seen in non-lesional MS white matter [normal appearing white matter-(NAWM)]. In contrast, MS lesions were classified as acute or chronic based on the presence of oil-red-O lipid filled macrophages and the amount of demyelination and haematoxylin-stained cellularity at the lesion border. An acute MS lesion consisted of many lipid-filled macrophages demonstrating an active area of demyelination of axonal fibers and a defined border (Fig. 1D). However, in a chronic lesion, no lipid-filled macrophages were present and the lesion area was completely demyelinated [28]. The acute lesion borders were marked on the adjacent sections of the very same sample and used for subsequent immunofluorescent staining. An antibody staining against calnexin (Fig. 1), an inflammatory endothelial cell marker, which we had previously shown to be elevated in brain endothelial cells of MS patients [29] was used as a guide for ER localization.

The SnPC of the Parkinsonian and control midbrain was identified based on the presence, of large (~50μm) neuromelanin containing bodies in Nissl-stained sections. (Fig. 2G and G1) Consecutive tissue sections were selected for the triple immunolabelling where cellular profiles of putative dopaminergic neurons were identified in non-neurodegenerative controls and their lesions in the diseased brain tissue samples, respectively. In frontal temporal cortex of AD and corresponding control brains, amyloid-β immunostaining was used to characterise deposits of misfolded proteins (Fig. 3P and R). Lower cervical sections selected from ALS spinal cord and the corresponding control tissues were contrasted with Cresyl violet (Fig. 4D and D1) to identify and locate motor neurons in the grey matter of the ventral horn and guide orientation and selection of subsequent tissue sections to be probed by specific antibodies against STING and toxic protein aggregates (TDP-43) in Fig. 4.

STING expression is elevated in neurodegenerative diseases in endothelial and neural cells

We found that STING is expressed predominantly in endothelial cells of brain capillaries and neuronal cell bodies of the pathological brain tissue samples. In the acute subcortical white matter of MS brain, there was evidence of abundant STING presence in cell bodies (Fig. 1). High levels of STING immunostaining showed colocalization with putative pyramidal cells in grey matter of the frontotemporal cortex of AD patients (Fig. 3), in the SnPC of PD (Fig. 2) and in putative motor neurons of the ALS spinal cord sections (Fig. 4). Activated microglia and astrocytes also demonstrated elevated STING in the cerebral cortex of AD patients of both familial and sporadic cases (Fig. 3 D-I), but only in moderation. In general, the intensity of STING staining in these former cells was less prominent compared to that of neurons (Fig. 3 A-C) and endothelial cells (Fig. 3 J-L). Misfolded protein plaques and neurons containing protein aggregates showed high level of STING immunofluorescent signal (Fig. 3 P-R). In contrast, STING expression in the control tissues was much less evident in all cell types in specific regions associated with of all four neurodegenerative diseases. In this study, we have demonstrated that neurons, which contain protein aggregates in multiple proteopathies (PD, AD, ALS) and the neuroinflammatory condition MS, are highly STING immuno-positive (Fig. 1-4) and are often localised in association with activated

microglia, astrocytes and endothelial cells (Fig. 3). In contrast, equivalent regions of non-neurodegenerative control CNS tissue showed quiescent STING immunosignal (Fig. 1, 2 and 3). We provide the first demonstration that four main neurodegenerative diseases have increased STING in specific cell types within different CNS areas associated with the pathology.

We observed that STING immuno-positive neuronal cell bodies were prevalent within the region of the SnPC of the PD brain tissue and demonstrated colocalization with putative dopaminergic neurons possessing intense a-synuclein staining (Fig. 2). The SnPC region was confirmed by the presence of neuromelanin in the neuronal cell bodies in Nissl-stained sections (Fig. 2 G and G1). Only a few highly STING positive neuronal cell bodies were observed in the associated brain region of the age matched control tissue sections (Fig. 2 D-F1) in contrast to the Parkinson's midbrains, where STING was highly prevalent and demonstrated strong colocalization with α-synuclein (Fig. 2. A-C1). Frontal-temporal cortical sections from AD patients were used for double immunostaining and localization of STING was confirmed in distinct neural cell types in the brain tissue. High intensity STING immunosignal was obvious in NeuN positive presumed neuronal cell bodies (Fig. 3A-C) and brain endothelial cells identified by morphological features of cross sections of brain vasculature in the cortical regions used for the histopathological examination (Fig. 3J-L). Cell specific markers for distinguishing glial cell subtypes; astrocytes (GFAP) and microglia (CD68), (also labels monocytes and macrophages) were double stained with STING to assess their localization in various CNS cell types (Fig. 3D-I). Both glial cell populations showed low intensity STING signal suggesting reduced STING activity in these cell types compared to neurons or brain endothelial cells. Interestingly, in grey matter, intense GFAP staining was seen in the pathological tissues, suggesting activated astrocytic processes are often associated with intense STING-positive neuronal cells in cortical parenchyma (Fig. 3D-F).

Disruption of mitochondrial respiration by palmitic acid

An observed consequence of neurodegeneration is the presence of damaged mitochondria, due to leakage of electrons from the electron transport chain (ETC) that interact with molecular oxygen and generate reactive oxygen species (ROS). These free radicals can damage mitochondria leading to release and damage of mitochondrial DNA, which is 100 times more susceptible to damage than nuclear DNA [30]. Such DNA could act as an activator of the cGAS/STING pathway. Therefore, we measured the oxygen consumption of mitochondria in hCMEC/D3s treated with and without PA, a known inducer of ROS. The electron transport chain uncoupler, FCCP was used to induce maximal ETC activity. FCCP is a potent uncoupler of mitochondrial oxidative phosphorylation. Actimycin A was used as a complex III inhibitor and negative control of respiration (Fig. 5A). Antimycin A induces a rapid loss in mitochondrial membrane potential, and a collapse of oxidative phosphorylation. Palmitic acid treatment reduced mitochondrial function by increasing oxygen consumption rates in hCMEC/D3s proportionally with PA concentration (10-100 μM) (Fig. 5B). Mitochondrial oxidative function is required to transform the energy of nutrients into a proton gradient pump used to make ATP via the ETC. The real-time OCR was increased in the presence of PA compared to basal respiration and appeared to supersede

the maximal respiratory capacity observed from the oxygen consumption after FCCP stimulation, which is known to be a strong indicator of mitochondrial energetic dysfunction [31].

Palmitic acid caused dsDNA leakage into the cytosol of hCMEC/D3s

To determine if PA induces DNA release from stressed hCMEC/D3s, we used PicoGreen as a marker of dsDNA, which is known to visualise dsDNA in non-permeabilised cells [26]. Our results showed that hCMEC/D3s treated with concentrations of PA (100-400μM) caused DNA leakage into the cytosol of the cells (Fig. 6). In untreated hCMEC/D3s, the intense blue fluorescence staining of nuclear DAPI can be seen coinhabiting the nucleus with the PicoGreen (dsDNA). There is very little evidence of dsDNA staining in the cytosol of untreated cells (Fig. 6, E). Palmitic acid is known to trigger nuclear [32] and mitochondrial [33] DNA damage. Leakage of such DNA into the cell's cytosol is known to activate cGAS [34, 35].

Thresholded quantitative colocalization analysis revealed a positive PA concentration-dependent co-occurrence between PicoGreen (dsDNA) and Mito Tracker Red (*mt*) in Fig. 6. ly, a plot of the simple spatial overlap of the dsDNA and *mt* probes (represented by overlapping pixels) indicated a significant positive relationship between the pixel's co-occurrence (dsDNA=*mt*) and the concentration of PA administered (a regression test; P <0.05; (Fig. 6Q). A regression test of Mander's coefficient M1 (the fraction of signal overlap between dsDNA (green) and *mt* (red)), significantly increased correspondingly with the concentrations of PA the cells were exposed to (regression test; P <0.05; Fig. 6R). This supports the notion that an increase in cytosolic dsDNA is associated with PA treatment. In contrast, a regression test of Mander's coefficient M2 (the fraction of signal overlap between *mt* (red) and dsDNA (green)), did not demonstrate a significant relationship with PA concentration (P >0.05) in Fig. 6R. This data suggests that the amount of *mt* that relates to dsDNA did not change as would be expected, as the proportion of *mt* in a cell should not have been affected by PA concentration (see details in Supplementary Table 3-6). In addition, cytosolic pixel intensity analysis also demonstrated that in the hCMEC/D3s cells dsDNA increased with PA concentration, as shown in Fig. 6 S-V.

Palmitic acid and cGAS activates the STING-TBK1 pathway and induces hCMEC/D3 inflammation

Having observed STING levels in the CNS microvascular endothelial cells of patients with different NDs, we wished to determine if the metabolic-stress induced fatty acid PA altered protein levels downstream in the STING signalling pathway in hCMEC/D3s. PA is known to be elevated in the brain of patients with Parkinson's [36] and Alzheimer's diseases [37] and serum of MS [38] and blood cells of ALS patients [39]. We treated hCMEC/D3s with PA at concentrations ranging from 1 - 400 mM. We observed that 100 mM PA had a significant effect of increasing the levels of STING in hCMEC/D3s (Fig. 7A) and 50 mM PA raised cGAS expression significantly (Fig. 7 B). The higher treatment doses of PA (200-400 mM) had minimal effect on STING and cGAS protein levels. Increased expression of ICAM on brain endothelial cells was observed in fresh-frozen post-mortem tissue from patients with neuroinflammatory diseases [40, 41]. As the downstream signaling molecule TBK-1 and the transcription factor pIRF3 of the STING pathway in part is known to bind to the ICAM gene promoter and induce ICAM expression on aortic

endothelial cells leading to increased cell attachment [33], we further investigated whether PA increased these downstream signaling molecules and subsequently ICAM expression and IFN-b on hCMEC/D3s. Here we observed a dose-dependent response to PA, which resulted in an increase in TBK-1, pIRF3, ICAM expression and IFN-b level in hCMEC/D3s (Fig. 7 C-F).

Activation of type I IFN expression in hCMEC/D3s

To investigate the innate immunity of hCMEC/D3s in response to PA-induced mitochondrial stress and STING activation, the capability of IFN-b release from cells was examined under specific agonist stimulation with PA. Saturated fatty acids such as PA have been implicated in inducing STING in endothelial cells [33] and STING in turn can activate a type I IFN responses [42], but the direct effect of PA on IFN-b in brain endothelia is unclear. As shown in Fig. 7 F, after treatment with PA, hCMEC/D3s released IFN-b in a dose dependent fashion. The reduced detection of IFN-b in the media of cells treated with 400 mM PA may reflect the reduced cell viability after such treatment.

Discussion

In this study, we have observed increased expression of STING in the CNS microvasculature and neuronal cells of individuals with various NDs. We show that elevated levels of STING are in close proximity to the buildup of protein aggregates such as TDP-43 in ALS, a-synuclein in PD and amyloid-β plaques in AD in a variety of neural cell types. The role of the cGAS-STING pathway in the human brain is only beginning to be explored in terms of a protective or pathological consequence. Recent evidence has revealed that STING signalling drives neuroinflammation in traumatic brain injury [43]. A downstream implication of STING activation is the production of type I IFNs. Elevated levels of type I IFNs have been found in brain post-mortem tissues of human AD [15], PD [44], and in ALS myeloid cells [45]. Further evidence that STING plays a role in neuroinflammation arises from STING knockout models, which have shown that elimination of STING alleviates some disease pathology in PD mice models [46]. What was striking is the particularly strong STING expression observed in endothelial cells in disease tissues compared to age matched non-neurodegenerative control CNS tissue. STING expression is known to occur in both normal and diseased tissue and may be important in anti-tumor development. Endothelial cells are the main producers of Type I IFNs [47], which raises the questions, are the CNS endothelia producing Type I IFNs in response to STING activation, and what is eliciting the increased STING production?

It was of interest to observe the colocalization of pathological protein aggregates near elevated STING expression in neural cells (Fig. 2, 3 and 4), which may be a reflection of ER and mitochondrial stress on the cells induced by toxic protein build up. In some other diseases such as arterial hypertension ER, mitochondrial stress and accumulation of protein aggregates have all been implicated in activation of STING [48]. In PD, overexpressed STING has been seen in the SnPC of patients and might be an important in PD pathogenesis [49]. In our human CNS tissues, we did not monitor IFN levels in these tissues so do not know if interferons were subsequently generated. In the AD tissue, STING was detected predominantly

in NeuN positive cortical neurons, putative pyramidal cells, but less evident in GFAP positive astrocytes or in CD68 positive microglia in AD tissue. This is despite a recent transgenic mouse model of AD reporting that enhancement of the cGAMP-STING pathway leads to the upregulation of microglia TREM2, which in turn suppresses amyloid-β-related neuropathology [50].

In the *in vitro* arm of this study, PA was used as an agonist of neuroinflammation, since PA and other saturated free fatty acids are associated with neurodegenerative processes [51]. In our study, PA-treatment of hCMEC/D3s led to the escape of dsDNA into the cytosol of cells (Fig. 6E-H), which is known to act as a ligand for the activation of DNA sensor cGAS [2]. The aim was not to address whether the detected cytosolic DNA originates from damaged mitochondria or nuclear DNA. However, analysis of the DAPI staining indicated that the nuclei staining was consistent across treatments (data not shown), indicating unlikely leakage of dsDNA from the nucleus. Others have investigated this in human aortic endothelial cells (HAECs), in which the source of the DNA appeared to be predominantly mitochondrial [33, 52, 53]. Subsequent STING activation was associated with an increase TBK-1 production (Fig. 7 C) and more pIRF3 (Fig. 7 E). Once pIRF3 enters the cell nucleus, it can bind to various gene promoters and enhance the expression of a number of downstream inflammatory factors in the cells (e.g. INF-b and ICAM-1). We detected that PA-activation of hCMEC/D3s led to increased ICAM expression on the cell surface, confirming the association between pIRF3 and ICAM expression, recently observed by Mao and colleagues [33]. We also observed that PA-treated endothelial cells released IFN-b in a dose dependent manner. Interestingly, endothelial cells in the presence of IFN-b become less permeable and increase the levels of tight junction proteins [54]. It remains to be investigated if the release of IFN-b by endothelial cells is a means to stabilize the BBB upon STING activation. STING signalling is associated with worsened neurodegenerative disease in mice [46, 55, 56] and our histology studies in human subjects (Fig. 1-4) appear to confirm these animal observations.

Our detection of STING activation in the brain endothelial cells of neurogenerative patients may also be a marker of Type-1 IFN release, notably IFNb. While IFNb therapies are of benefit to a cohort of MS patients, some MS patients treated with IFNb have been observed to go on to develop PD-like symptoms [57]. Recent studies have shown that the IFN pathway is grossly upregulated in clinical AD [58] and PD [44]. Although IFNs are well known for their anti-viral properties, they can exert anti-inflammatory effects [59]. An increase in STING-mediated INF-b expressed by BBB endothelial cells could indicate a reduction in immune cell trafficking or an attempt to retain BBB integrity between the blood and CNS and not necessarily neuroinflammation [60]. However, somewhat paradoxically, in earlier studies INFb was shown in murine models of experimental autoimmune encephalomyelitis (EAE) to decrease the abundance of adhesion molecules on brain capillaries such as ICAM-1 and VCAM-1 [61]. In our study, we saw an increase in ICAM and IFN-b expression of hCMEC/D3s treated with PA, possibly via IRF3 phosphorylation and nuclear translocation of this transcriptional inducer of IFN-b and ICAM. A previous study [33] showed that PA-treated endothelial cells led to ICAM induced expression via the STING-pIRF3 pathway. Overall, in neurodegeneration, activation of the cGAS STING pathway could be through viral DNA, but could also be through self DNA (nuclear or mitochondrial) triggered by pathological protein fibrils (Fig. 8) or lipid toxicity. Viral aetiologies for NDs have received a lot of attention, and these data don't rule out viral DNA

as activating the cGAS STING pathway in NDs. But our data in general support a self DNA story (cellular stress and DNA release caused by build up of fibrillar proteins), or, from PA- metabolic activation of human brain endothelial cells.

Conclusions

Several NDs lead to neural cell damage and a reduced ability to remove damaged mitochondria in response to stress, resulting in STING-mediated inflammation. Our observations suggest that both the brain microvasculature and neurons in AD, PD, ALS and MS demonstrate a common increase in cGAS-STING pathway signalling compared to age-matched control tissue. We have demonstrated that nuclear or mitochondrial DNA escape induced by PA-mediated inflammation is recognised by cGAS leading to activation of the STING-TBK-1 signaling pathway and increased expression of important inflammatory factors.

Abbreviations

AD = Alzheimer's disease; ALS = amyotrophic lateral sclerosis; Ctx = cortex; FTCx = frontal-temporal cortex; MS = multiple sclerosis; PD = Parkinson's disease; PMD = post-mortem time; SnPC = substantia nigra pars compacta; WM = white matter; NAWM = normal appearing white matter; PA = palmitic acid; cGAS = cyclic GMP-AMP synthase; STING stimulatory interferon gene; TBK-1 = TANK-binding kinase 1; ICAM 1 = intracellular adhesion molecule 1; pIRF3 = phosphorylated interferon regulatory factor 3; IFNβ = interferon β; *mt* = mitochondria; NDs = neurodegenerative diseases, ETC = electron transport chain, ROS = reactive oxygen species; BBB = blood brain barrier; IFNs = interferons; hCMEC/D3 = human cortical microvessels endothelial cells/D3; IFI16 = Interferon-gamma induced protein 16; Ab = β-amyloid protein; BSA = bovine serum albumin; TDP-43 = TAR DNA binding protein 43; FA = fatty acid; FAO = fatty acid oxidation; FCCP = carbonyl cyanide-4-(trifluormethoxy) phenylhydrazone; LM = linear regression models; LFN = lane normalization factor; SIM = structured illumination microscopy; OCR = real-time extracellular oxygen consumption

Declarations

Acknowledgements

The Queen Square Brain Bank for Neurological Disorders is supported by the Reta Lila Weston Institute of Neurological Studies, UCL Queen Square Institute of Neurology. The MS Society Tissue Bank, funded by the Multiple Sclerosis Society of Great Britain and Northern Ireland, registered charity 207495. We are

thankful for the generous donations from Sheryl Moorey's family and Grahame Brown to aid the further understanding of MS disease.

Funding

This study was funded by UCB Pharma (AM, ASF, PE) and by the Northcott Devon Medical Foundation (Grant 5002) to PE and NJG.

Availability of data and materials

All data generated or analyzed during this study are included in this published article [and its supplementary information files].

Authors' contributions

The experiments were performed by ASF, MS, CL. The tissue samples from patients were collected under the supervision JN & JEH. ASF, PE, NJG, AM, MS & CL designed the study and wrote the manuscript with editing assistance provided by JW, JEH and JN.

Competing interests

The authors report no competing interests.

Consent for publication

All authors have read the manuscript and consent of its publication.

Ethics approval and consent to participate

MS brain tissue and control samples, with associated clinical and neuropathological data, were supplied by the MS Society Tissue Bank, multicenter ethics number (08/MRE 09/31). An additional MS sample, ALS and control post-mortem tissues were obtained from the NeuroResource tissue bank, and ALS, AD and control samples were from the Queen Square Brain Bank for Neurological Disorders. Ethical approvals for these studies were obtained from the tissue banks, which are both based at the UCL Queen Square Institute of Neurology, London and have the Tissue Bank NHS Research Ethics Committee approval 18/LO/0721 from the London - Central Research Ethics Committee.

References

1. Reinert LS, Lopusna K, Winther H, Sun C, Thomsen MK, Nandakumar R, Mogensen TH, Meyer M, Vaegter C, Nyengaard JR, et al: **Sensing of HSV-1 by the cGAS-STING pathway in microglia orchestrates antiviral defence in the CNS**. Nat Commun 2016, **7**:13348.
2. Zierhut C, Funabiki H: **Regulation and Consequences of cGAS Activation by Self-DNA**. Trends Cell Biol 2020, **30**:594–605.

3. Gutowski NJ, Ferecsko AS, Smallwood M, Holley J, Newcombe J, Moore A, Eggleton P: **Human neurodegenerative CNS tissues show robust expression of cGAS-STING pathway components in association with inflammation**. Eur J Neurology 2019, **26**:717–717.
4. Ahmad L, Zhang SY, Casanova JL, Sancho-Shimizu V: **Human TBK1: A Gatekeeper of Neuroinflammation**. Trends Mol Med 2016, **22**:511–527.
5. Oakes JA, Davies MC, Collins MO: **TBK1: a new player in ALS linking autophagy and neuroinflammation**. Mol Brain 2017, **10**:5.
6. Chen Q, Sun L, Chen ZJ: **Regulation and function of the cGAS-STING pathway of cytosolic DNA sensing**. Nat Immunol 2016, **17**:1142–1149.
7. Decout A, Katz JD, Venkatraman S, Ablasser A: **The cGAS-STING pathway as a therapeutic target in inflammatory diseases**. Nat Rev Immunol 2021, **21**:548–569.
8. Blank T, Prinz M: **Type I interferon pathway in CNS homeostasis and neurological disorders**. Glia 2017, **65**:1397–1406.
9. Kraus J, Oschmann P: **The impact of interferon-beta treatment on the blood-brain barrier**. Drug Discov Today 2006, **11**:755–762.
10. Li J, Wang Y, Wang X, Ye L, Zhou Y, Persidsky Y, Ho W: **Immune activation of human brain microvascular endothelial cells inhibits HIV replication in macrophages**. Blood 2013, **121**:2934–2942.
11. Lin JY, Kuo RL, Huang HI: **Activation of type I interferon antiviral response in human neural stem cells**. Stem Cell Res Ther 2019, **10**:387.
12. Crow MK, Ronnblom L: **Type I interferons in host defence and inflammatory diseases**. Lupus Sci Med 2019, **6**:e000336.
13. Hoffmann HH, Schneider WM, Rice CM: **Interferons and viruses: an evolutionary arms race of molecular interactions**. Trends Immunol 2015, **36**:124–138.
14. Nazmi A, Field RH, Griffin EW, Haugh O, Hennessy E, Cox D, Reis R, Tortorelli L, Murray CL, Lopez-Rodriguez AB, et al: **Chronic neurodegeneration induces type I interferon synthesis via STING, shaping microglial phenotype and accelerating disease progression**. Glia 2019, **67**:1254–1276.
15. Taylor JM, Moore Z, Minter MR, Crack PJ: **Type-I interferon pathway in neuroinflammation and neurodegeneration: focus on Alzheimer's disease**. J Neural Transm (Vienna) 2018, **125**:797–807.
16. Jauhari A, Baranov SV, Suofu Y, Kim J, Singh T, Yablonska S, Li F, Wang X, Oberly P, Minnigh MB, et al: **Melatonin inhibits cytosolic mitochondrial DNA-induced neuroinflammatory signaling in accelerated aging and neurodegeneration**. J Clin Invest 2020, **130**:3124–3136.
17. Dunphy G, Flannery SM, Almine JF, Connolly DJ, Paulus C, Jonsson KL, Jakobsen MR, Nevels MM, Bowie AG, Unterholzner L: **Non-canonical Activation of the DNA Sensing Adaptor STING by ATM and IFI16 Mediates NF-kappaB Signaling after Nuclear DNA Damage**. Mol Cell 2018, **71**:745–760 e745.
18. Jeffries AM, Marriott I: **Human microglia and astrocytes express cGAS-STING viral sensing components**. Neurosci Lett 2017, **658**:53–56.

19. Engin AB: *What Is Lipotoxicity? BT-Obesity and Lipotoxicity;*. Springer International Publishing: Cham,Switzerland; 2017.
20. Kim DW, Glendining KA, Grattan DR, Jasoni CL: **Maternal Obesity in the Mouse Compromises the Blood-Brain Barrier in the Arcuate Nucleus of Offspring**. Endocrinology 2016, **157**:2229–2242.
21. Rhea EM, Salameh TS, Logsdon AF, Hanson AJ, Erickson MA, Banks WA: **Blood-Brain Barriers in Obesity**. AAPS J 2017, **19**:921–930.
22. Patil S, Chan C: **Palmitic and stearic fatty acids induce Alzheimer-like hyperphosphorylation of tau in primary rat cortical neurons**. Neurosci Lett 2005, **384**:288–293.
23. Freitas HR, Ferreira GDC, Trevenzoli IH, Oliveira KJ, de Melo Reis RA: **Fatty Acids, Antioxidants and Physical Activity in Brain Aging**. Nutrients 2017, **9**.
24. Brodowicz J, Przegalinski E, Muller CP, Filip M: **Ceramide and Its Related Neurochemical Networks as Targets for Some Brain Disorder Therapies**. Neurotox Res 2018, **33**:474–484.
25. Patil S, Balu D, Melrose J, Chan C: **Brain region-specificity of palmitic acid-induced abnormalities associated with Alzheimer's disease**. BMC Res Notes 2008, **1**:20.
26. Ashley N, Harris D, Poulton J: **Detection of mitochondrial DNA depletion in living human cells using PicoGreen staining**. Exp Cell Res 2005, **303**:432–446.
27. Dunn KW, Kamocka MM, McDonald JH: **A practical guide to evaluating colocalization in biological microscopy**. Am J Physiol Cell Physiol 2011, **300**:C723-742.
28. Li H, Newcombe J, Groome NP, Cuzner ML: **Characterization and distribution of phagocytic macrophages in multiple sclerosis plaques**. Neuropathol Appl Neurobiol 1993, **19**:214–223.
29. Jung J, Eggleton P, Robinson A, Wang J, Gutowski N, Holley J, Newcombe J, Dudek E, Paul AM, Zochodne D, et al: **Calnexin is necessary for T cell transmigration into the central nervous system**. JCI Insight 2018, **3**.
30. Kim HR, Won SJ, Fabian C, Kang MG, Szardenings M, Shin MG: **Mitochondrial DNA aberrations and pathophysiological implications in hematopoietic diseases, chronic inflammatory diseases, and cancers**. Ann Lab Med 2015, **35**:1–14.
31. Brand MD, Nicholls DG: **Assessing mitochondrial dysfunction in cells**. Biochem J 2011, **435**:297–312.
32. Beeharry N, Lowe JE, Hernandez AR, Chambers JA, Fucassi F, Cragg PJ, Green MH, Green IC: **Linoleic acid and antioxidants protect against DNA damage and apoptosis induced by palmitic acid**. Mutat Res 2003, **530**:27–33.
33. Mao Y, Luo W, Zhang L, Wu W, Yuan L, Xu H, Song J, Fujiwara K, Abe JI, LeMaire SA, et al: **STING-IRF3 Triggers Endothelial Inflammation in Response to Free Fatty Acid-Induced Mitochondrial Damage in Diet-Induced Obesity**. Arterioscler Thromb Vasc Biol 2017, **37**:920–929.
34. Kato K, Omura H, Ishitani R, Nureki O: **Cyclic GMP-AMP as an Endogenous Second Messenger in Innate Immune Signaling by Cytosolic DNA**. Annu Rev Biochem 2017, **86**:541–566.

35. Wu J, Sun L, Chen X, Du F, Shi H, Chen C, Chen ZJ: **Cyclic GMP-AMP is an endogenous second messenger in innate immune signaling by cytosolic DNA**. Science 2013, **339**:826–830.
36. Fabelo N, Martin V, Santpere G, Marin R, Torrent L, Ferrer I, Diaz M: **Severe alterations in lipid composition of frontal cortex lipid rafts from Parkinson's disease and incidental Parkinson's disease**. Mol Med 2011, **17**:1107–1118.
37. Fraser T, Tayler H, Love S: **Fatty acid composition of frontal, temporal and parietal neocortex in the normal human brain and in Alzheimer's disease**. Neurochem Res 2010, **35**:503–513.
38. Armon-Omer A, Waldman C, Simaan N, Neuman H, Tamir S, Shahien R: **New Insights on the Nutrition Status and Antioxidant Capacity in Multiple Sclerosis Patients**. Nutrients 2019, **11**.
39. Henriques A, Blasco H, Fleury MC, Corcia P, Echaniz-Laguna A, Robelin L, Rudolf G, Lequeu T, Bergaentzle M, Gachet C, et al: **Blood Cell Palmitoleate-Palmitate Ratio Is an Independent Prognostic Factor for Amyotrophic Lateral Sclerosis**. PLoS One 2015, **10**:e0131512.
40. Turowski P, Adamson P, Greenwood J: **Pharmacological targeting of ICAM-1 signaling in brain endothelial cells: potential for treating neuroinflammation**. Cell Mol Neurobiol 2005, **25**:153–170.
41. Moore L, Eggleton P, Smerdon G, Newcombe J, Holley JE, Gutowski NJ, Smallwood M: **Engagement of people with multiple sclerosis to enhance research into the physiological effect of hyperbaric oxygen therapy**. Mult Scler Relat Disord 2020, **43**:102084.
42. Hu X, Peng X, Lu C, Zhang X, Gan L, Gao Y, Yang S, Xu W, Wang J, Yin Y, Wang H: **Type I IFN expression is stimulated by cytosolic MtDNA released from pneumolysin-damaged mitochondria via the STING signaling pathway in macrophages**. FEBS J 2019, **286**:4754–4768.
43. Chin AC: **PERK-STING Signaling Drives Neuroinflammation in Traumatic Brain Injury**. J Neurosci 2020, **40**:2384–2386.
44. Main BS, Zhang M, Brody KM, Ayton S, Frugier T, Steer D, Finkelstein D, Crack PJ, Taylor JM: **Type-1 interferons contribute to the neuroinflammatory response and disease progression of the MPTP mouse model of Parkinson's disease**. Glia 2016, **64**:1590–1604.
45. McCauley ME, O'Rourke JG, Yanez A, Markman JL, Ho R, Wang X, Chen S, Lall D, Jin M, Muhammad A, et al: **C9orf72 in myeloid cells suppresses STING-induced inflammation**. Nature 2020.
46. Sliter DA, Martinez J, Hao L, Chen X, Sun N, Fischer TD, Burman JL, Li Y, Zhang Z, Narendra DP, et al: **Parkin and PINK1 mitigate STING-induced inflammation**. Nature 2018, **561**:258–262.
47. Demaria O, De Gassart A, Coso S, Gestermann N, Di Domizio J, Flatz L, Gaide O, Michielin O, Hwu P, Petrova TV, et al: **STING activation of tumor endothelial cells initiates spontaneous and therapeutic antitumor immunity**. Proc Natl Acad Sci U S A 2015, **112**:15408–15413.
48. Cicalese SM, da Silva JF, Priviero F, Webb RC, Eguchi S, Tostes RC: **Vascular Stress Signaling in Hypertension**. Circ Res 2021, **128**:969–992.
49. Zhao M, Wang B, Zhang C, Su Z, Guo B, Zhao Y, Zheng R: **The DJ1-Nrf2-STING axis mediates the neuroprotective effects of Withaferin A in Parkinson's disease**. Cell Death Differ 2021, **28**:2517–2535.

50. Xu Q, Xu W, Cheng H, Yuan H, Tan X: **Efficacy and mechanism of cGAMP to suppress Alzheimer's disease by elevating TREM2**. Brain Behav Immun 2019, **81**:495–508.
51. Gonzalez-Giraldo Y, Forero DA, Echeverria V, Garcia-Segura LM, Barreto GE: **Tibolone attenuates inflammatory response by palmitic acid and preserves mitochondrial membrane potential in astrocytic cells through estrogen receptor beta**. Mol Cell Endocrinol 2019, **486**:65–78.
52. Hinkle JT, Patel J, Panicker N, Karuppagounder SS, Biswas D, Belingon B, Chen R, Brahmachari S, Pletnikova O, Troncoso JC, et al: **STING mediates neurodegeneration and neuroinflammation in nigrostriatal alpha-synucleinopathy**. Proc Natl Acad Sci U S A 2022, **119**:e2118819119.
53. Standaert DG, Childers GM: **Alpha-synuclein-mediated DNA damage, STING activation, and neuroinflammation in Parkinson's disease**. Proc Natl Acad Sci U S A 2022, **119**:e2204058119.
54. Kraus J, Ling AK, Hamm S, Voigt K, Oschmann P, Engelhardt B: **Interferon-beta stabilizes barrier characteristics of brain endothelial cells in vitro**. Ann Neurol 2004, **56**:192–205.
55. Masanneck L, Eichler S, Vogelsang A, Korsen M, Wiendl H, Budde T, Meuth SG: **The STING-IFN-beta-Dependent Axis Is Markedly Low in Patients with Relapsing-Remitting Multiple Sclerosis**. Int J Mol Sci 2020, **21**.
56. Yu CH, Davidson S, Harapas CR, Hilton JB, Mlodzianoski MJ, Laohamonthonkul P, Louis C, Low RRJ, Moecking J, De Nardo D, et al: **TDP-43 Triggers Mitochondrial DNA Release via mPTP to Activate cGAS/STING in ALS**. Cell 2020, **183**:636–649 e618.
57. Manouchehrinia A, Constantinescu CS: **Cost-effectiveness of disease-modifying therapies in multiple sclerosis**. Curr Neurol Neurosci Rep 2012, **12**:592–600.
58. Roy ER, Wang B, Wan YW, Chiu G, Cole A, Yin Z, Propson NE, Xu Y, Jankowsky JL, Liu Z, et al: **Type I interferon response drives neuroinflammation and synapse loss in Alzheimer disease**. J Clin Invest 2020, **130**:1912–1930.
59. Axtell RC, Steinman L: **Type 1 interferons cool the inflamed brain**. Immunity 2008, **28**:600–602.
60. Benveniste EN, Qin H: **Type I interferons as anti-inflammatory mediators**. Sci STKE 2007, **2007**:pe70.
61. Floris S, Ruuls SR, Wierinckx A, van der Pol SM, Dopp E, van der Meide PH, Dijkstra CD, De Vries HE: **Interferon-beta directly influences monocyte infiltration into the central nervous system**. J Neuroimmunol 2002, **127**:69–79.

Figures

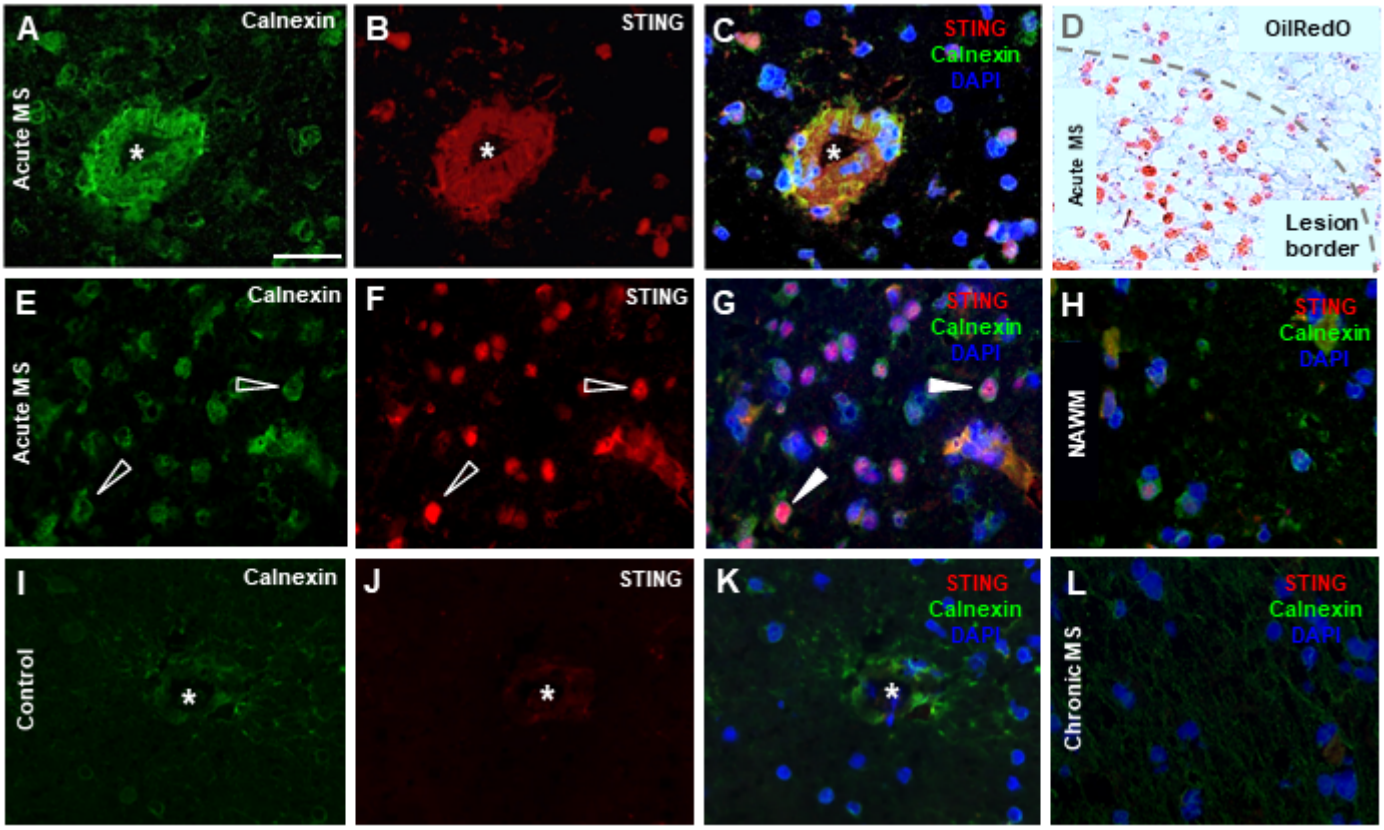

Figure 1

Representative immunofluorescent labelling of STING in acute, chronic, NAWM MS brain tissue and control WM. (**A-C**) Increased levels of STING were present in the endothelial cells, which were heavily stained for calnexin, of brain microvasculature, marked with asterisk in the acute MS lesion. (**D**) Lesions were assessed with the lipid staining oil-red-O adjacent to immune stained sections. (**E** and **F**) STING-positive neuronal cell bodies (open arrowhead) were seen in the proximity of the subcortical white/grey matter border in the acute MS lesion (filled arrow head in **G**), whilst MS NAWM (**H**), chronic (**L**) and non-MS control tissue (**I-K**) demonstrated much lower STING immunopositivity and lack of colocalization with the calnexin positive structures. Both the chronic MS lesions and NAWM from the acute MS brain demonstrated low levels of STING immunosignal in endothelial cells (not shown). Scale bar represents 50μm.

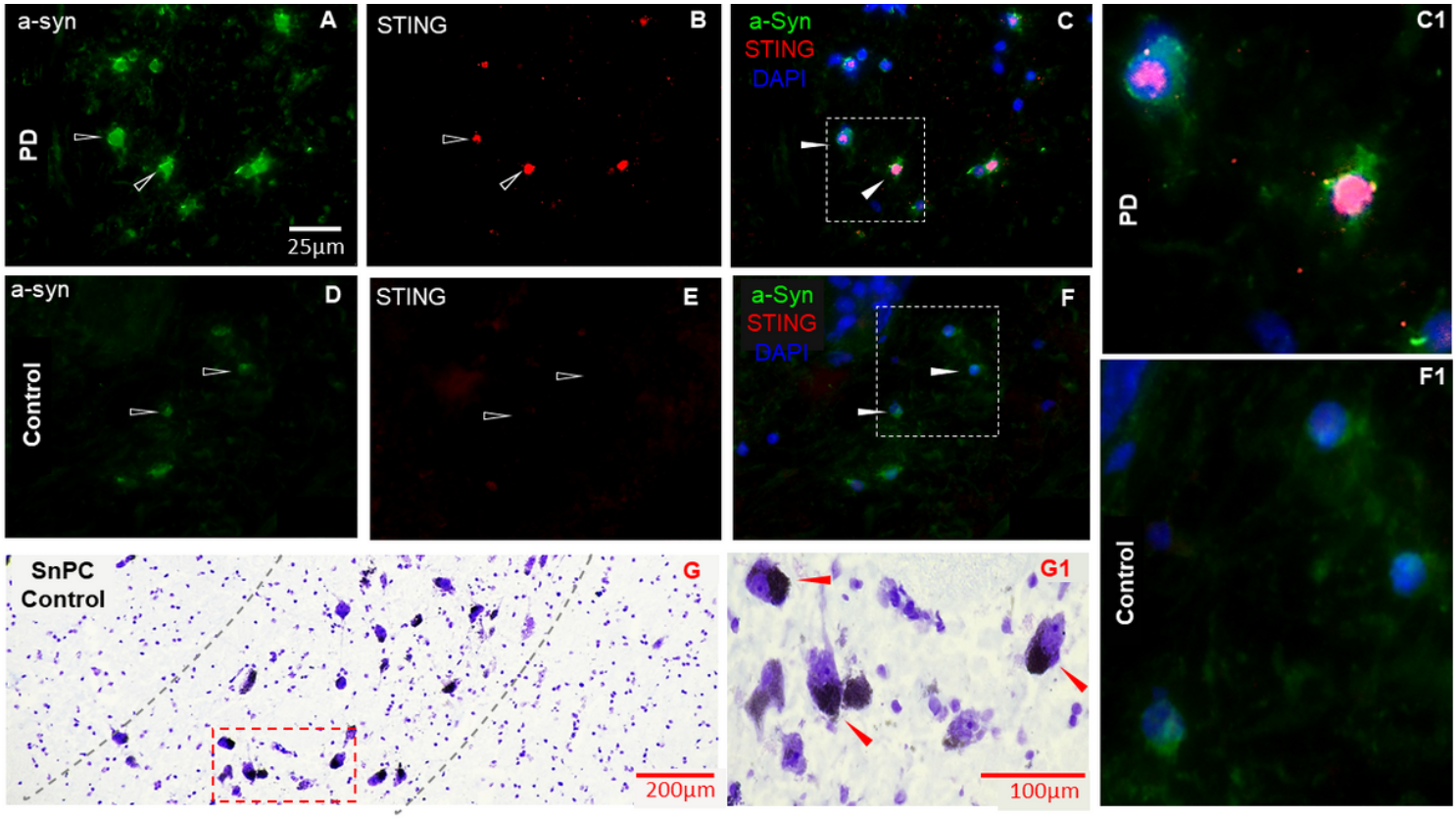

Figure 2

Immunofluorescent staining of representative tissue sections in PD and control SnPC. Increased STING immunosignal was present in highly α-synuclein positive cell bodies in PD brain (open arrowhead in **A** and **B** respectively) and demonstrated strong colocalization (filled arrowhead in **C**, enlarged in **C1**) while control tissue (**D-F**) showed minimal STING signal (**E**) with little α-synuclein present (**D**) thus the lack of colocalization (filled arrowhead in **F**, enlarged in **F1**). SnPC was identified using Nissl-stained midbrain sections (**G**), based on the presence, of neuromelanin containing large (~50µm) somatic profiles, as putative dopaminergic neurons (red arrow heads in **G1**) in both the non-neurodegenerative control tissue (**G1**) and PD brain samples (not shown). Scale bar for A is representative for A-F.

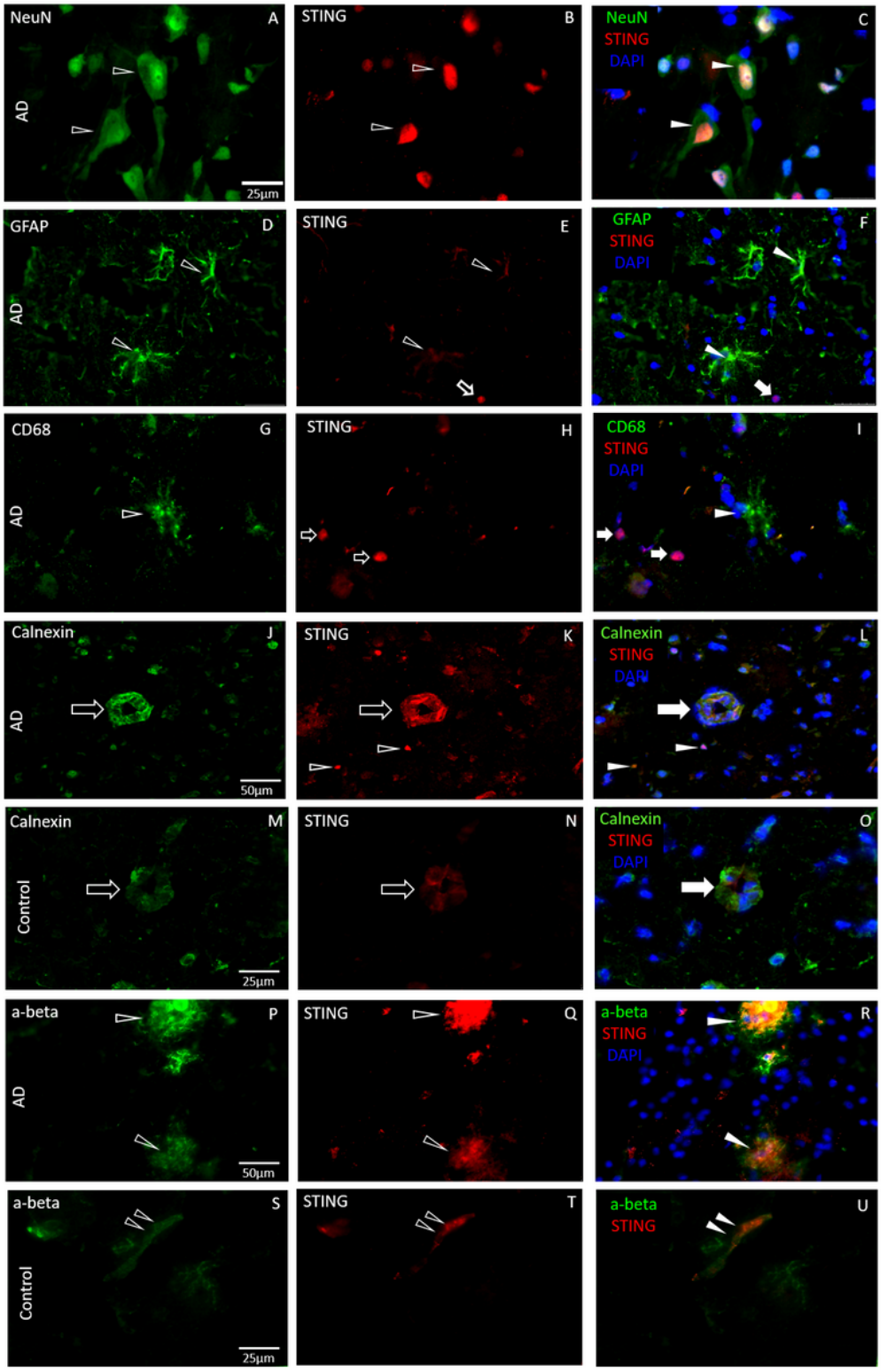

Figure 3

STING immunostaining in neural cells in association with amyloid-β in AD and control brain parenchyma. NeuN labelled putative pyramidal cells (open arrow head in **A**) show intense STING immune signal (**B** and **C**) while astrocytes (GFAP), (**D** and **F**) and microglia (CD68), (**G** and **I**) demonstrated weak STING positivity (open arrow head in **E** and **H**, respectively). NeuN positive cells contain high levels of STING (filled arrow in **C**) compared to the GFAP expressing astrocytes and CD68-positive myeloid cells (filled

arrow head in **F** and **I**, respectively) that designate reduced STING positivity. Increased STING positivity was present in the endothelial cells (open arrow in **J** , **K** and filled arrow in **L**) in the frontal-temporal cortex of the AD brain in contrast to blood vessels of the control tissue with decreased STING levels (open arrow in **M**, **N** and filled arrow in **O**). Cortical amyloid-β depositions demonstrated robust STING presence and strong colocalization with the pathological plaques (open arrow heads **P**, **Q** and filled arrow heads in R). Only low level of STING was detected in amyloid-β depositions found occasionally in the brain microvasculature of age matched control cortex (double open arrow heads **S**, **T**) with no obvious abnormal amyloid-pathology in the same structure (double filled arrow heads in **U**). Neuronal cell bodies were strongly labelled with STING in AD brain (open arrows in **H** and arrowheads in **K**) and colocalized with DAPI (filled arrows in **I** and arrow heads in **L**).

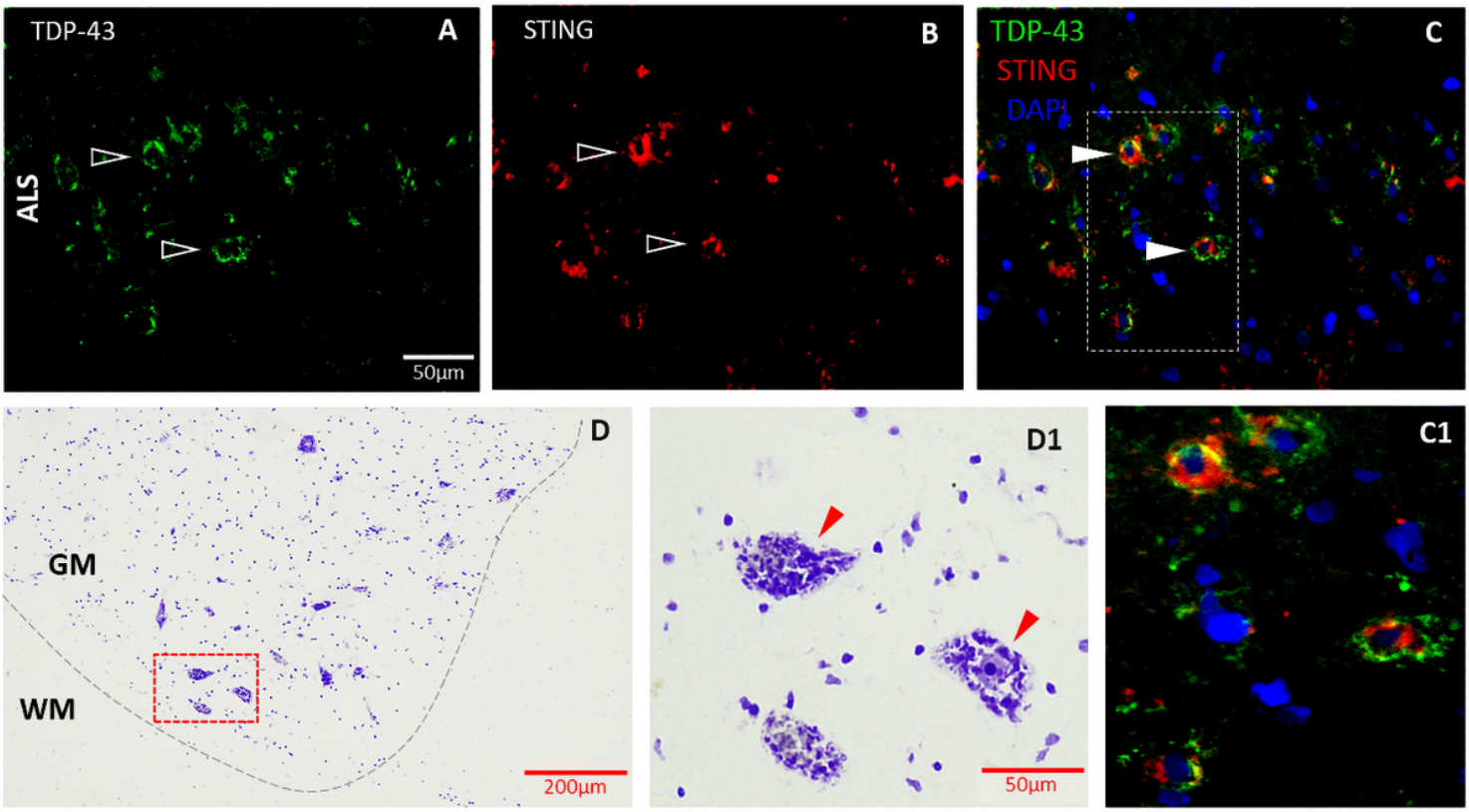

Figure 4

Representative examples of immunohistopathological examination of STING in motor neurons. Tissue samples from the lower cervical segment of the spinal cord of a sporadic ALS patient (**A-C** and **C1**). STING showed colocalization with TDP-43 large cell bodies (filled arrow head in **C**, enlarged in **C1**) of presumed motor neurons. Adjacent to immunolabelled sections Nissl contrast staining was used for identifying motor neurons (a rrow head in **D1**) in both control (**D**, **D1**) and ALS spinal cord samples (not shown). GM; grey matter, WM; white matter.

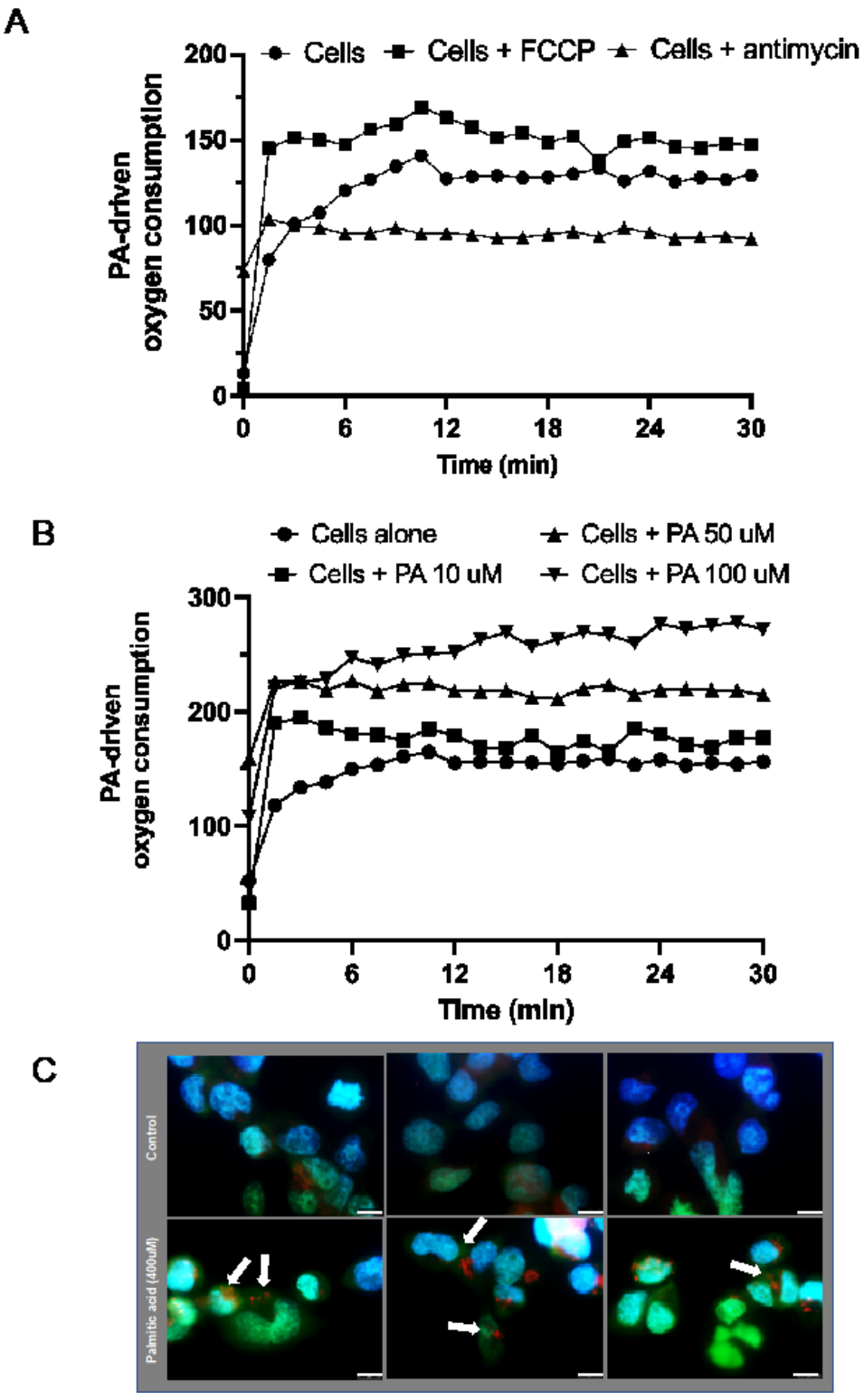

Figure 5

Increased oxygen consumption in PA treated hCMEC/D3s. (**A**) Representative traces of OCR of hCMEC/D3s in the presence or absence of FCCP or antimycin. (**B**) Dose dependent increase in hCMEC/D3s OCR with exposure to increasing concentrations of PA. Extracellular oxygen consumption signal was measured at 1.5 min intervals for 30 minutes at Ex/Em = 380/650 nm.

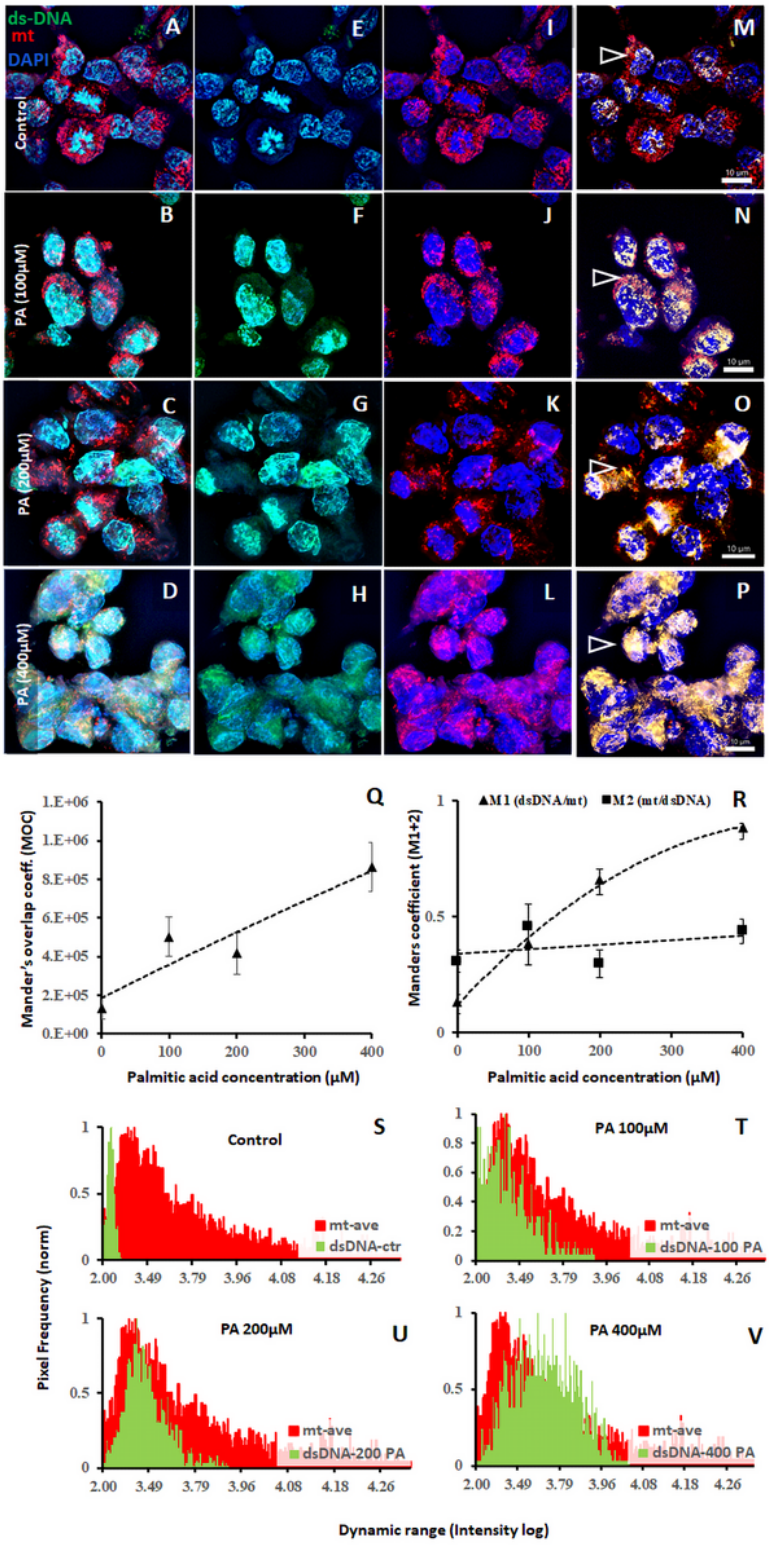

Figure 6

Mitochondrial DNA release and colocalization analysis of mitochondria (*mt*) and dsDNA in PA treated hCMEC/D3s. (**A-D**) Far-left column - Representative images of hCMEC/D3s stained with dsDNA marker PicoGreen, DAPI (blue) and the *mt*-specific marker Mito-Tracker Red. (**E-H**) Centre-left column- hCMEC/D3s cells showing tracks with dsDNA marker PicoGreen and DAPI (blue). (**I-L**) Centre-right column - hCMEC/D3s cells showing tracks labelled with DAPI (blue) and Mito-Tracker Red. (**M-P**) Far-right

column - hCMEC/D3 cells showing leakage of dsDNA (depicted by yellow pixels), which increases in the cell's cytosol with increasing PA concentration. Open arrow heads (**M-P**) indicate examples where the increase in dsDNA in the cytosol is apparent thus colocalization (yellow area) between dsDNA and *mt* is evident. (**Q**) Illustrates the positive correlation of the increasing co-occurrence between *mt* and dsDNA; across PA treatment. (**R**) Coefficient M1 (dsDNA/*mt*) indicates that the fraction of dsDNA that overlaps with *mt* increased with PA concentration, revealing a clear dose-dependent relationship (*n*=6-8). Coefficient M2 (*mt*/dsDNA) demonstrates that the fraction of *mt*overlapping with dsDNA did not change across PA concentrations (*n*=6-8). (**S-V**) Cytosolic pixel intensity analysis showed a shift of the 'green' peak to the right, supporting that dsDNA increased with PA concentration. Pixel profiles were extracted from where the open arrow heads are indicated (**M-P**). Pixel frequency is normalised between 0 and 1, and *mt* represents a logged average from across PA treatments.

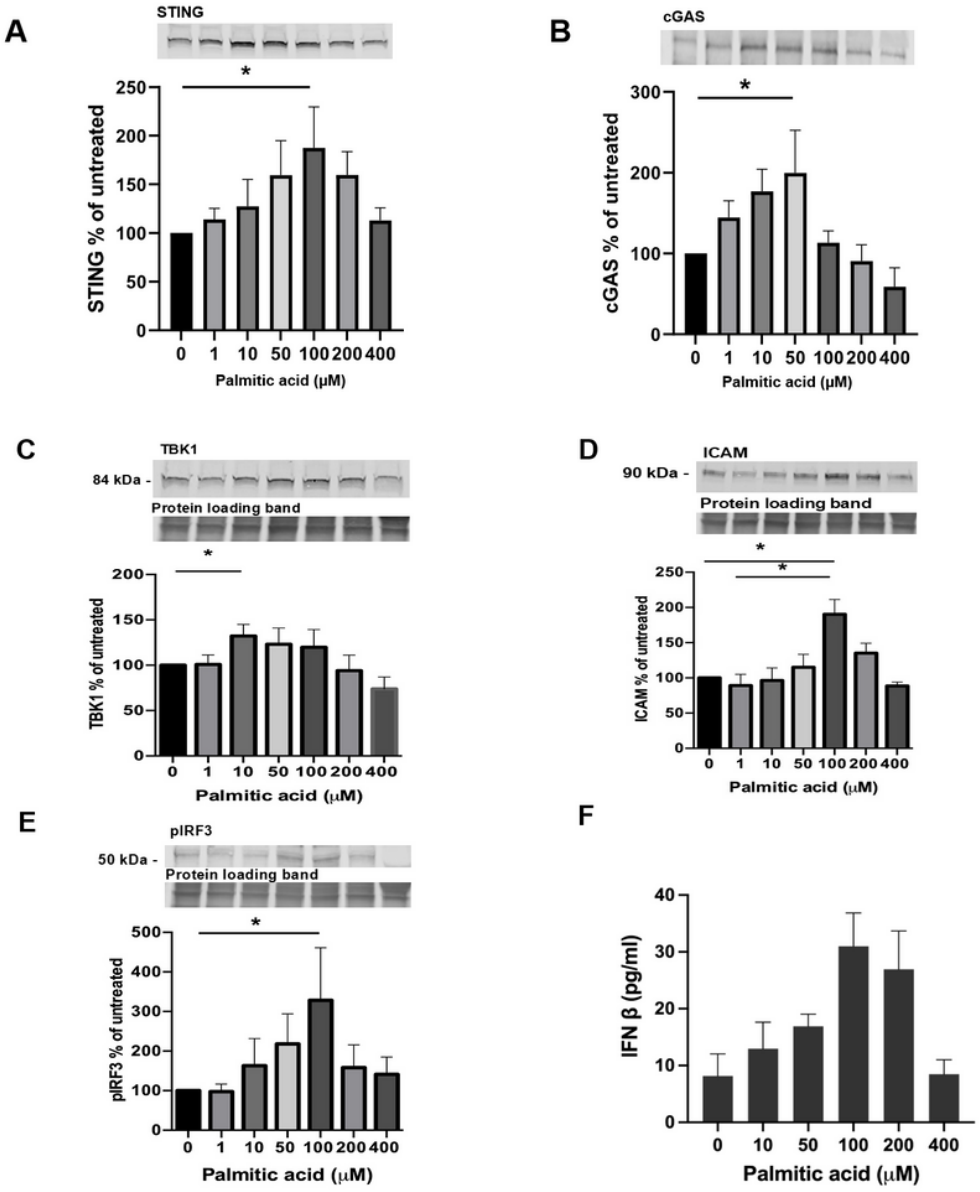

Figure 7

Effect of PA treatment on cGAS-STING signaling and down-stream ICAM and INF-b production in hCMEC/D3s. (**A-B**) Effect of palmitic acid treatment on cGAS and STING. Dose response effect of PA on (**C**) TBK-1, (**D**) pIRF3 and (**E**) ICAM production, *n*= 5-6 experiments/condition. (**F**) Release of IFN-b from cells *n*=5 replicates. Data are expressed as mean % change ± SEM from untreated cells. Mann Whitney * denotes *p*-values <0.05.

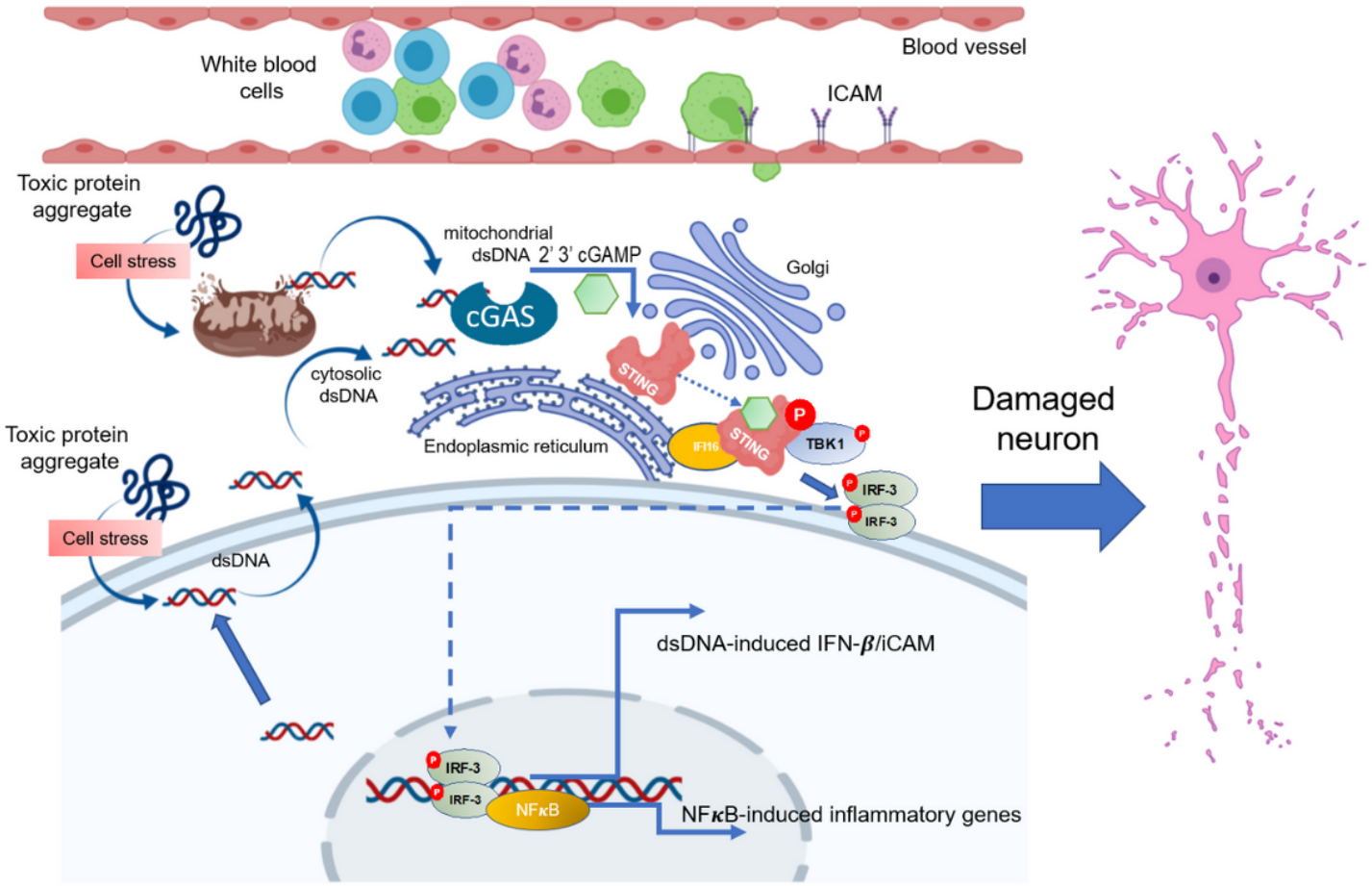

Figure 8

Schematic diagram of activation of cGAS-STING pathway in the CNS. Cytosolic DNA is recognised by cGAS leading to formation of cGAS-DNA complex. This leads to synthesis of 2' 3'-cGAMP – STING ligand. Activated STING translocates from the ER to the proximity of the Golgi, where STING is post-translationally modified (palmitoylated and phosphorylated) by TBK-1. This provokes STING to recruit IRF3, leading to IRF3 phosphorylation and dimerisation and the pIRF dimer travels to the nucleus to drive expression of both type I interferons and ICAM expression, as well as NFk-B inflammatory genes. This diagram was created with BioRender.com.

Supplementary Files

This is a list of supplementary files associated with this preprint. Click to download.

- SupplementaryMaterial.docx